RSC Advances

PAPER

View Article Online
View Journal | View Issue

Open Access Article. Published on 02 October 2023. Downloaded on 11/4/2025 12:38:13 AM.
This article is licensed under a Creative Commons Attribution-NonCommercial 3.0 Unported Licence.

Check for updates

Cite this: *RSC Adv.*, 2023, **13**, 28843

Preparation of γ-phase pigment Red 170 through hydrothermal treatment and kaolin coating modification

Dongjun Lv,*[ab] Xiaolei Zhang,*[ab] Zilong Zhang,[a] Jiahui Zhang,[ab] Yi Li,[a] Ruobing Qi,[a] Yuxue Zhang[a] and Jing Tang[a]

Received 19th July 2023
Accepted 26th September 2023

DOI: 10.1039/d3ra04857h

rsc.li/rsc-advances

Research on the dynamics of crystal transformation can guide production practices and improve the coloration performance of pigment Red 170. As one of the most important azo dyes, the low hiding power, inferior weather resistance, thermal instability, and low flowability of pigment Red 170 limit its applications. To enhance these properties, it is essential to modify the surface of the pigment. Herein, the crystal transformation and isothermal crystallisation kinetics of colour index (C.I.) pigment Red 170 during a hydrothermal process were studied through X-ray powder diffraction. During isothermal crystallisation, the Avrami indexes (*n*) were 2.65 and 3.01, and the kinetic rate constants (*K*) were 6.02×10^{-6} and 8.34×10^{-6} at 140 and 150 °C, respectively. The apparent activation energies (*E*) are 10.42 and 24.31 kcal mol^{-1} for the incubation period and total transition, respectively. Pigment Red 170 completely transferred from an α-phase to γ-phase upon hydrothermal treatment at 140 and 150 °C for 180 and 90 min, respectively. The effects of heat treatment temperature and time on the colour hue, tinctorial strength, flowability, particle size and distribution, contact angle, thermal stability, and morphology of pigment Red 170 were investigated. In addition, kaolin was used as an inorganic additive to modify γ-phase pigment Red 170. After hydrothermal treatment and kaolin modification, C.I. pigment Red 170 had a small particle size and exhibited a narrow size distribution and improved hydrophilicity. The γ-phase pigments had a tinctorial strength of 189.5%. The flowability and thermal stability of the kaolin-modified pigment were also enhanced. This study promotes the development of pigments with enhanced colour properties, thermal stability, and processability.

Introduction

Organic pigments have been extensively used in coatings,[1,2] inks,[3–5] cosmetics,[6] and plastics[7] owing to their solvent resistance,[8] high tinctorial strength, excellent transparency, colour brilliance, weather resistance, thermal stability, and low toxicity.[9–13] An azo dye is the most well-known organic pigment, accounting for more than 60% of the total production of organic pigments.[14,15] As one of the most important azo dyes, pigment Red 170 demonstrates good colour tone, high colour brightness, and high tinctorial strength. However, its low hiding power, inferior weather resistance, thermal instability, and low flowability[16,17] limit its applications. To enhance these properties, it is essential to modify the surface of pigment Red 170.[18,19] The main modification methods of pigment Red 170 include surfactant modification, inorganic core inclusion, and polymer coating.[20–23] Wu *et al.*[24] prepared a new quaternary ammonium salt containing siloxane groups to modify the surface of pigment Red 170. The modified pigment had a small particle size, good wettability, high flowability, and excellent dispersion stability. Xiao *et al.*[25] coated the pigment Red 170 surface with hydrated alumina obtained from the hydrolysis of $Al_2(SO_4)_3$, significantly improving the UV diffuse reflection, high-temperature resistance, and solvent resistance. Zhang *et al.*[26] modified pigment Red 170 by preparing carbon black nucleated by an anti-coupling method. After modification, the average particle size of the pigment decreased and the particle size distribution narrowed. Moreover, the pigment colouring strength, heat resistance, flowability, and water dispersion improved. Cao *et al.*[27] used micro-silicon powder absorbed with silane coupling agents (KH550, KH560 and KH570, *etc.*) to react with a diazo salt solution. Pigment Red 170 was produced *in situ* through the reaction between diazo and the coupling agent, and the micro-silicon powder coating improved the thermal stability and light stability of the pigment. Zhang *et al.*[28] employed reversible addition–fragmentation chain transfer (RAFT) polymerisation to synthesise a random copolymer of 2-(dimethylamino)ethyl methacrylate (DMAEMA), poly(ethylene glycol)

[a]*Department of Chemical Engineering, School of Chemistry and Chemical Engineering, De Zhou University, Dezhou, 253023, China. E-mail: lvdongjun@dzu.edu.cn; zhangxl@dzu.edu.cn*

[b]*Shandong Universities Engineering Research Center of Integrated Circuits Functional Materials and Expanded Applications, Dezhou, 253023, China*

© 2023 The Author(s). Published by the Royal Society of Chemistry

Open Access Article. Published on 02 October 2023. Downloaded on 11/4/2025 12:38:13 AM. This article is licensed under a Creative Commons Attribution-NonCommercial 3.0 Unported Licence.

methyl ether methacrylate (PEGA), and methyl methacrylate (MMA) or butyl acrylate (BA) with a trithiocarbonate-reactive end group. These cationic macromolecular RAFT agents (macro-RAFT) were subsequently adsorbed on the surface of monodispersed colloidal pigment Red 170 particles at pH 5. The resulting organic pigment hybrid latex particles demonstrated excellent dispersion stability during freeze–thaw cycles, storage, and pH variation.

Pigment Red 170 has an α-phase, a β-phase, and a γ-phase;[29] the α-phase and γ-phase are homogeneous heterocrystals. The α-phase of pigment Red 170 is unstable and must be converted to the more stable β-phase and γ-phase for practical applications.[30] Therefore, it is essential to optimise the processing conditions to ensure complete transformation. The research on the dynamics of the crystal transformation can guide the production practice and improve the performance of traditional azo pigments. In addition to the phase transformation, hydrothermal treatment and coating modification can also improve the properties of pigments.

In this study, the crystal transformation and isothermal crystallisation kinetics of pigment Red 170 during 140 and 150 °C hydrothermal treatments were examined by X-ray powder diffraction. The time required for the complete transformation from the α-phase to γ-phase was determined, and the isothermal crystallisation behaviour was analysed by the Avrami equation. The Avrami index (n), the crystallisation kinetic rate constant (K), and the apparent activation energy (E) were calculated to determine the growth mode of the pigment Red 170 and provide a theoretical basis for the application of pigment Red 170. The effects of the heat treatment temperature, heat treatment time, and kaolin nucleation modification on the colour hue, tinctorial strength, flowability, particle size and distribution, hydrophilicity, thermal stability, and the morphology of pigment particles were studied systemically during the phase transformation.

Experimental

Materials

4-Aminobenzamide (Red Base DB-70, 99.0%) was provided by Shandong Sunshine Pigment Co., Ltd. 3-Hydroxy-*N*-(2-ethoxyphenyl)-2-naphthalenecarboxamide (Naphthol AS-PH, 98.5%) was obtained from Shandong Andie New Material Co., Ltd. Kaolin (99.0%) was purchased from BASF SE. Concentrated hydrochloric acid (36.0%), sodium nitrite, glacial acetic acid, and sodium hydroxide were supplied by Tianjin Kemiou Chemical Reagent Co., Ltd. All other chemicals were of analytical grade and used as received without further purification.

Methods

First, a diazonium salt solution was prepared. 4-Aminobenzamide (13.7 g, 0.100 mol) was dissolved in cold deionised water (100 mL). HCl (36%, 13.7 g) was added, and the mixture was stirred for 20 min. Next, crushed ice was added to adjust the temperature to 0 °C. Then, a 30% sodium nitrite solution (7.0 g) was added dropwise within 5 min under stirring, and the temperature was controlled at 10–15 °C for 1 h. After the reaction, sulfamic acid was introduced to react with the excessive sodium nitrite to avoid the generation of nitrous acid, which might affect the subsequent coupling reaction.

Next, the coupling component was prepared by the following procedure. Naphthol AS-PH (32.5 g, 0.105 mol) was dissolved in deionised water (200 mL) in a 500 mL beaker. Then, sodium hydroxide (10.5 g) was added to the beaker while stirring. Next, the solution was heated to 65 °C until the Naphthol AS-PH was dissolved completely.

To prepare the modified pigment, sodium hydroxide (3.0 g), glacial acetic acid (13.5 g), and crushed ice were dissolved in deionised water (250 mL) in a 1 L beaker. Then, a buffer solution (pH 3.9) was added dropwise to the diazonium salt solution with a peristaltic pump within 15 min. During the reaction, the temperature and pH were maintained at 8–10 °C and 1.9, respectively. Finally, the coupling agent was added dropwise to the diazonium salt solution with a peristaltic pump over 120 min. During the reaction, the temperature was maintained between 10 and 25 °C, and the pH was 4.6. The reaction was continued for 10 min, and the product was filtered and washed to obtain wet filtered cake.

For the hydrothermal treatment and kaolin modification, the wet filter cake (28.0 g) was combined with kaolin (0.35 g) in deionised water (100 mL) in a 200 mL beaker. Next, the suspension was magnetically stirred for 20–30 min until well mixed. The pH of the mixture was adjusted to 3.8 with glacial acetic acid, and stirring was continued for 10 min. Then, deionised water (20 mL) was added, and the solution was poured into an autoclave. The autoclave was heated in an oven at 140 °C or 150 °C for various treating times. Finally, after cooling, the treated pigment solution was filtered, washed with deionised water until a neutral pH, and dried at 80 °C. The preparation process and synthesis routes of the modified pigments are illustrated in Fig. 1 and Scheme 1.

Instruments and equipment

The colours of the pigments were assessed using an International Commission on Illumination (CIE) 1976 L^* a^* b^* system. Colour measurements were performed using an X-rite 8400 automatic colorimeter (X-RITE, USA). The colour strength and flowability were determined according to the Chinese National Standard (GB/T 1708-79) and the National Industry Standard of the People's Republic of China (HG/T 3854-2006), respectively.

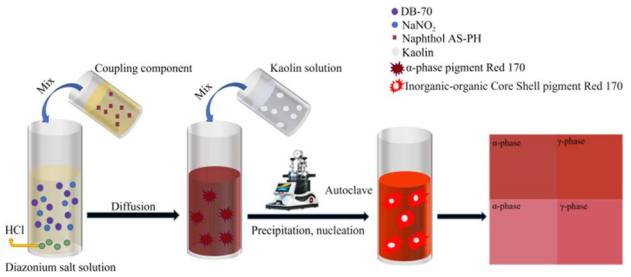

Fig. 1 Synthesis process for γ-phase pigment Red 170.

 © 2023 The Author(s). Published by the Royal Society of Chemistry

Open Access Article. Published on 02 October 2023. Downloaded on 11/4/2025 12:38:13 AM.
This article is licensed under a Creative Commons Attribution-NonCommercial 3.0 Unported Licence.

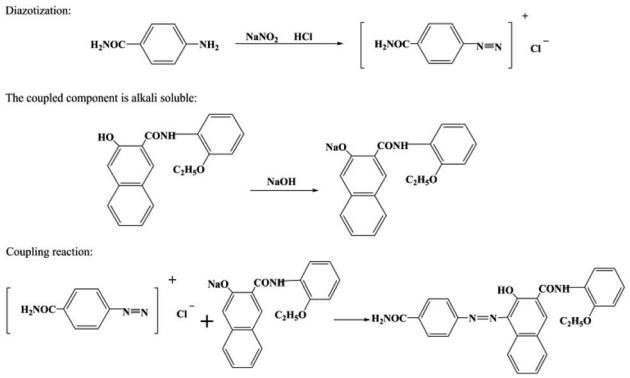

Scheme 1 Synthetic route of pigment Red 170.

The particle size distributions were determined using a Mastersizer 2000 particle size analyser (Malvern, UK) after sonicating an aqueous pigment suspension for 15 min. The morphologies of the pigments were observed by scanning electron microscopy (SEM). SEM was conducted at a 5 kV voltage and 6 mm working distance with an SE2 detector (Merlin Compact, Zeiss Corporation, Oberkochen, Germany). The pigment was sputtered with gold before the SEM observation. The crystalline phases of the pigment were determined by X-ray diffractometry (XRD, D8A, Bruker, Germany) with a Cu Kα X-ray source generated at 40 kV and 40 mA. Powder X-ray diffraction data of the pigment was recorded over a 2θ range of 5–40° at room temperature. The chemical structures of the hydrothermal-treated and kaolin-modified pigments were determined by Fourier transform-infrared spectroscopy (FT-IR, Nicolet 380, Thermo Electron Corporation, USA). The wettability of the pigment was determined by measuring the water contact angles of a pellet sample (EasyDrop, KRUSS GmbH, Germany). For water contact angle measurement, the samples were first tableted in an infrared tablet press to obtain a sheet. The time between drop deposition and measurement was 2 s, and the volume of drops measured in each experiment was 3 μL.

Results and discussion

XRD

XRD was performed to determine the crystal structure, and the results are shown in Fig. 2. Fig. 2 lists the integral strength values of the pigments obtained by hydrothermal treatments at 140 and 150 °C at different times and by kaolin modification. The untreated pigment had characteristic diffraction peaks at $2\theta = 5.3°$, 7.6°, 8.2°, 11.7°, 15.9°, and 18.8°.

After the hydrothermal treatment at 140 and 150 °C, the pigment diffraction peaks became stronger, suggesting improved crystallinity. When the treatment time was 180 min at 140 °C (90 min at 150 °C), new diffraction peaks appeared at $2\theta = 7.2°$, 11.3°, 12.9°, 18.1°, and 30.8°. In addition, for the pigments modified by kaolin, new diffraction peaks related to kaolin emerged at 12.3° and 24.9°. By comparing the characteristic peaks of the non-nucleated and nucleated pigments, the peak positions were the same, indicating that kaolin modification did not change the crystalline phase. However, the diffraction peak intensities of the kaolin-modified pigments at $2\theta = 7.2°$, 11.3°, 18.1°, 20.2°, and 25.6° were lower than those of the unmodified pigments, indicating that the inorganic nucleus kaolin inhibited the growth of pigment crystal particles to some extent.

SEM

SEM was used to analyse the morphology of the untreated, hydrothermal-treated, and kaolin-modified pigments; the results are shown in Fig. 3. The particle size distribution of the untreated pigment Red 170 was not uniform, and distinct aggregated particles were observed. In the process of organic pigment preparation, particularly during insulation and drying, pigment particles tended to aggregate due to the intermolecular forces between them (such as hydrogen bonding, van der Waals force, *etc.*). As shown in Fig. 3a–c, the pigment particles grew gradually at 140 °C with the increase in the treatment time until forming rod particles. As shown in Fig. 3d, the particle size of the pigment after kaolin nucleation modification was small. In addition, compared with the untreated pigment, the

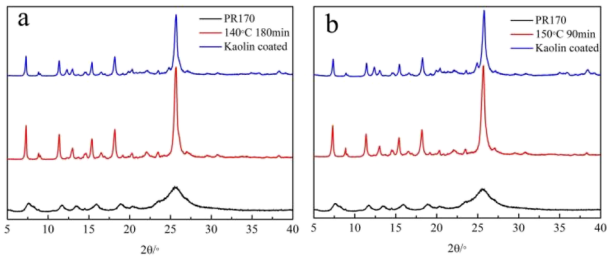

Fig. 2 XRD curves of unmodified (PR170), hydrothermal treatment pigment at 140 °C (a) and 150 °C (b), and coating modification pigment samples.

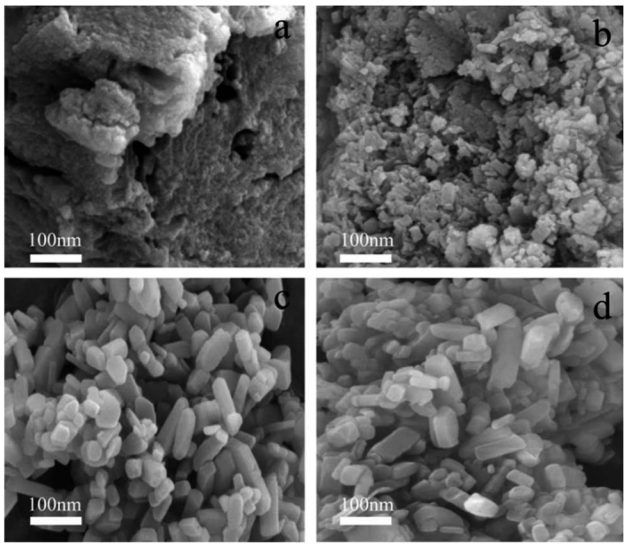

Fig. 3 SEM analysis of pigment treated under thermal treatment in water: (a) untreated, (b) 140 °C 60 min, (c) 140 °C 180 min, (d) kaolin coating modification.

Open Access Article. Published on 02 October 2023. Downloaded on 11/4/2025 12:38:13 AM.
This article is licensed under a Creative Commons Attribution-NonCommercial 3.0 Unported Licence.

hydrothermal-treated and kaolin-modified pigments had a regular rod-like shape. The above results indicated that the morphology and particle size of organic pigments were controlled to a certain extent by the hydrothermal treatment and kaolin modification.

Isothermal crystallisation kinetics

XRD is the most effective method to identify crystal phases and their percentages. Therefore, the pigment Red 170 was analysed by XRD to determine the percentages of the α-phase and γ-phase. The XRD patterns of pigment Red 170 at different temperatures are shown in Fig. 4, confirming the conversion from the α-phase to γ-phase.

The diffraction peaks of the α-phase and γ-phase of pigment Red 170 were generally overlapped. However, the α-phase had a weak peak in the 2θ range of 4°–6°, while this peak was absent in the γ-phase. Therefore, the diffraction peak at 2θ of 4°–6° and d value of 17.245 was selected to characterise the α-phase to achieve accurate diffraction intensity measurement and quantitative analysis. The intensity of this diffraction peak was defined as I_α. The diffraction intensity of a pure α-phase was measured by the same method and defined as $I_{\alpha P}$. The weight percentage of the α-phase (W_α (%)) in the mixture was calculated using $I_\alpha/I_{\alpha P}$. In the kinetic assay quantitative analysis, $I_{\alpha P}$ is a relative standard value and determined according to specific experimental conditions and methods. In this study, $I_{\alpha P}$ was measured under the same temperature, and the treated samples were obtained at different times, and the mean value of integral strength of untransformed samples was used as $I_{\alpha P}$.

The time-dependent crystallinity in pigment Red 170 isothermal crystallisation at different temperatures was determined; the results are presented in Tables 1, 2, and Fig. 5. According to Tables 1 and 2, at the same temperature, the isothermal crystallisation rate increased with the isothermal crystallisation time.

During the hydrothermal treatment, the phase transformation of pigment Red 170 occurs similarly to the crystallisation and partial solid reaction. The process involves the nucleation and growth of the crystal particle. Under isothermal conditions, the crystallisation rate conforms to the Avrami–Erofeev equation:[31]

$$W_r(t) = 1 - \exp(-kt^n) \tag{1}$$

A rate equation was obtained by taking the logarithm of both sides of eqn (1)

$$\ln(1 - W_r) = -Kt^n \tag{2}$$

After taking the logarithm of both sides of eqn (2) and (3) was derived.

$$\ln[-\ln(1 - W_r)] = n \ln t + \ln K \tag{3}$$

where $W_r(t)$ is the relative crystallinity at time t, K is the crystallisation kinetic rate constant, n is the Avrami index depending on the nucleation and growth processes. The n value is 3 or 4 for spherulite three-dimensional growth, 2 or 3 for flaky two-dimensional growth, and 1 or 2 for acicular one-dimensional growth.

The Avrami formula was used to analyse the apparent activation energy (E) of the transformation process:

$$t = t_0 \exp(E/RT) \tag{4}$$

where R is the gas constant (1.987 cal mol^{-1}), T is the transition temperature (K), t is the transition time (min), t_0 is a dependent constant.

To facilitate the calculation of E, eqn (4) is transformed to its logarithmic form:

$$\ln t = E/RT + \ln t_0 \tag{5}$$

According to eqn (5):

$$\ln t_1 - \ln t_2 = E/R(T_2 - T_1/T_1T_2) \tag{6}$$

Fig. 6 shows the plot of $\ln[-\ln(1 - W_r)]$ and $\ln t$. The linear relationship indicated that the isothermal crystallisation process of pigment Red 170 followed the Avrami equation. Table 3 lists the Avrami exponent (n), kinetic rate constant (K) obtained from the slope and intercept of the linear fitting, and correlation coefficient (r). The n value was between 2.65 and 3.01. By comparing with the relationship between the Avrami

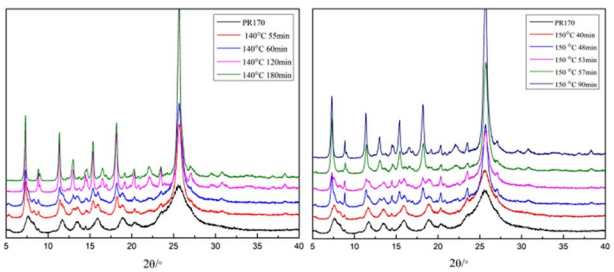

Fig. 4 X-ray powder diffraction pattern of α-phase to γ-phase crystal transition.

Table 1 Relationship between time and conversion rate at 140 °C

Time (min)	30	50	55	60	65	75	85	120	180
W_α (%)	100.0	100.0	81.9	73.1	18.0	11.2	5.7	4.1	1.8
W_γ (%)	0	0	18.1	26.9	82.0	88.8	94.3	95.9	98.2

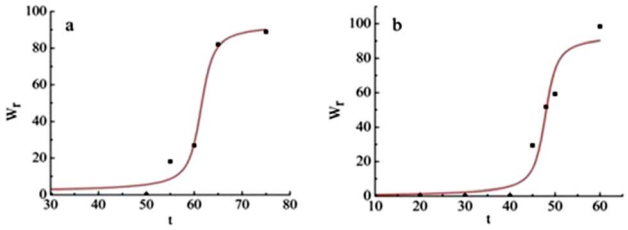

Fig. 5 Relative crystallinity *versus* time for pigment Red 170 crystallised at 140 °C (a) and 150 °C (b).

 © 2023 The Author(s). Published by the Royal Society of Chemistry

Open Access Article. Published on 02 October 2023. Downloaded on 11/4/2025 12:38:13 AM.
This article is licensed under a Creative Commons Attribution-NonCommercial 3.0 Unported Licence.

Table 2 Relationship between time and conversion rate at 150 °C

Time (min)	10	20	30	40	45	48	50	53	55	57	60	70	80	90
W_α (%)	100.0	100.0	100.0	100.0	70.6	48.3	40.8	39.0	21.6	12.7	1.6	1.5	0.9	0.3
W_γ (%)	0	0	0	0	29.4	51.7	59.2	61.0	78.4	87.3	98.4	98.5	99.1	99.7

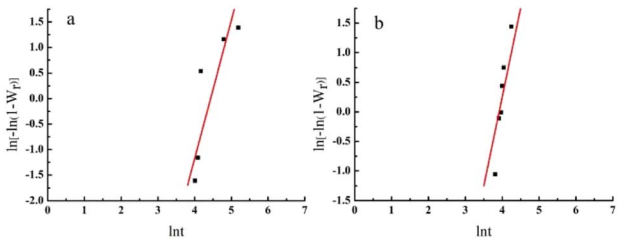

Fig. 6 Pigment Red 170 of ln[−ln(1 − W_r)] *versus* ln t for isothermal crystallization at 140 °C (a) and 150 °C (b) .

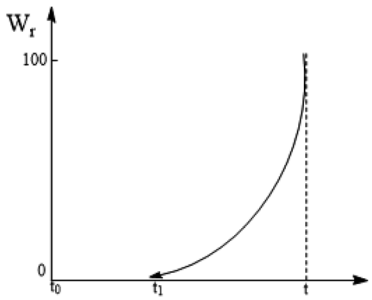

Fig. 7 Relationship between α-phase to γ-phase conversion rate and time.

Table 3 Kinetic parameters for isothermal crystallization of pigment Red 170

Temperature (°C)	n	ln k	K	r
$T_1 = 140$	2.65	−12.02	6.02×10^{-6}	0.9721
$T_2 = 150$	3.01	−11.70	8.34×10^{-6}	0.9666

Table 5 Incubation time and total transition time

Temperature (K)	Incubation period (t_{inc})	Total transition time (t_{tot})
$T_1 = 413$	50 min	180 min
$T_2 = 423$	40 min	90 min

index and crystallisation behaviour (Table 4), the growth mode of pigment Red 170 isothermal crystallisation was determined as three-dimensional spherulite growth.

Fig. 7 shows the relationship between the phase transformation rate and time. From initial t_0 to t_1, no crystal transformation was observed, corresponding to an incubation period. From t_1 to t, the α-phase gradually changed to the γ-phase until a complete transformation.

The Avrami formula was used to analyse the apparent activation energy (E) of the transformation process. The incubation time and total transition time data (Table 5) were substituted into eqn (6), and the apparent activation energy values were 10.42 and 24.31 kcal mol^{-1} for incubation period and total transition, respectively.

Colour properties and flowability

The colour performances of hydrothermal-treated (140 °C) and untreated pigment Red 170 (sample 6–1 in the flowing tables) are compared in Table 6. The contrast between the full shade and tint shade of the pigment treated at 140 °C is shown in Fig. 8. The maximum L value was obtained when the treatment time was 180 min. In addition, pigment Red 170 after the hydrothermal treatment showed high colour saturation, as evidenced by the large and positive c values. When the treatment time was 285 min, the resulting pigment had a strong yellow hue ($H = 37.80$) and high tinctorial strength (114.8%). The flowability of pigment increased gradually with the extension of time. Further, when the treatment time was 300 min, the resulting pigment had a maximum flowability (41 mm). The colouring strength of the hydrothermal-treated pigment was higher than that of the untreated pigment. At 140 °C for 180 min, the α-phase was completely converted to the γ-phase, and the tinctorial strength was 141.2%, and the flowability increased significantly.

When the treatment temperature was 150 °C, the colour performance of pigments is shown in Table 7. The contrast between the full shade and tint shade of the pigment treated at 150 °C is shown in Fig. 9. When the treatment times were 53, 75, and 85 min, the resulting pigments (Table 7, entries 7–8, 7–13, 7–14) had higher L and c values than the untreated pigment, suggesting higher lightness and colour saturation. When the treatment times were 50 and 60 min, the resulting pigments had strong yellow hues with H values of 30.73 and 31.08,

Table 4 Relationship between Avrami index and crystallization behavior

Growth pattern/nucleation pattern	Homogeneous nucleus	Heterogeneous nucleation
One-dimensional growth (acicular crystal)	$n = 1 + 1 = 2$	$n = 1 + 0 = 1$
Two-dimensional growth (sheet crystal)	$n = 2 + 1 = 3$	$n = 2 + 0 = 2$
Three-dimensional growth (spherical crystal)	$n = 3 + 1 = 4$	$n = 3 + 0 = 3$

Open Access Article. Published on 02 October 2023. Downloaded on 11/4/2025 12:38:13 AM.
This article is licensed under a Creative Commons Attribution-NonCommercial 3.0 Unported Licence.

Table 6 Effect of treating pigment by hydrothermal treatment at 140 °C

Time (min)	*L*	*a*	*b*	*c*	*H*	Tinctorial strength (%)	Flowability (mm)
—	45.94	48.57	25.60	54.91	27.79	100.0	26
30	44.52	50.26	27.67	57.40	28.78	137.1	26
50	43.50	49.62	32.08	59.15	32.80	173.2	27
55	42.65	50.39	31.58	59.42	32.10	182.5	27
60	44.01	53.40	33.07	62.78	31.93	189.5	28
20	44.75	55.12	32.63	64.03	30.85	163.6	35
180	47.69	53.08	24.53	58.48	24.82	141.2	36
240	47.20	54.46	28.76	61.60	27.78	131.6	37
255	44.77	56.47	33.78	65.69	31.87	124.9	39
270	46.04	54.47	30.09	62.24	28.91	116.7	40
285	45.42	55.80	32.83	64.51	37.80	114.8	40
300	47.25	54.00	27.29	60.51	26.79	104.4	41

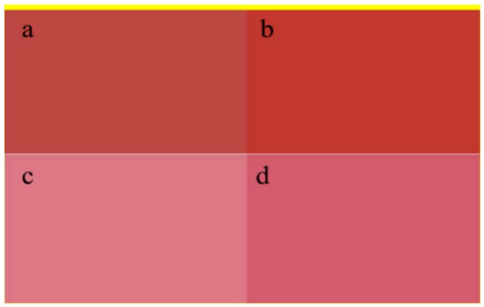

Fig. 8 Color comparison of the modified pigment by hydrothermal treatment at 140 °C between α-phase (a: full shade, c: tint shade) and γ-phase (b: full shade, d: tint shade).

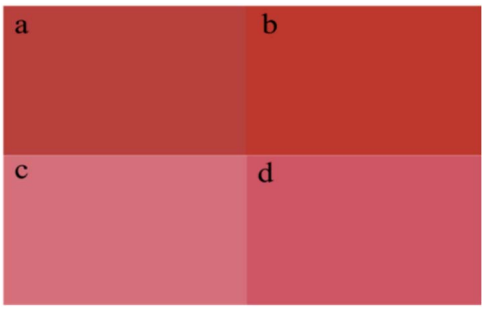

Fig. 9 Color comparison of the modified pigment by hydrothermal treatment at 150 °C between α-phase (a: full shade, c: tint shade) and γ-phase (b: full shade, d: tint shade).

respectively. The flowability of pigment increased gradually with the extension of the treatment time. Further, when the treatment time was 50 min, the resulting pigment had a maximum colour strength (179.5%). At 150 °C for 90 min, the α-phase was completely converted to the γ-phase, and the tinctorial strength was 140.6%, and the flowability increased significantly.

Next, the effect of coating modification on the properties of the pigment were studied (Table 8) in the presence of kaolin. The full shade and tint shade of pigments by kaolin modification are shown in Fig. 10. When the treatment temperature were 140 and 150 °C, the tinctorial strengths of the kaolin-modified pigments were slightly lower than that without kaolin and

Table 7 Effect of treating pigment by hydrothermal treatment at 150 °C

Time (min)	*L*	*a*	*b*	*c*	*H*	Tinctorial strength (%)	Flowability (mm)
—	45.94	48.57	25.60	54.91	27.79	100.0	26
10	42.63	48.55	26.80	55.46	28.86	99.6	26
20	45.80	48.18	24.08	53.86	26.62	99.8	26
30	44.18	49.05	27.76	56.37	29.45	100.2	27
40	45.46	49.66	28.32	57.19	29.64	110.8	28
45	46.74	49.21	25.43	55.39	27.33	140.3	28
48	46.42	52.24	29.98	60.30	29.67	153.9	29
50	45.65	52.20	31.13	60.84	30.73	179.5	29
53	49.41	50.04	29.98	58.42	30.79	161.0	29
55	45.75	52.12	30.57	60.48	30.28	148.8	30
57	44.48	53.06	30.39	61.21	29.63	147.7	31
60	45.04	52.91	31.87	61.79	31.08	147.2	31
65	45.97	54.67	30.64	62.67	29.27	147.1	32
75	46.23	54.78	30.14	62.53	28.82	146.9	33
85	46.16	55.05	30.50	62.93	28.99	144.1	34
90	45.43	54.15	30.26	62.07	29.03	140.6	35

 © 2023 The Author(s). Published by the Royal Society of Chemistry

Open Access Article. Published on 02 October 2023. Downloaded on 11/4/2025 12:38:13 AM.
This article is licensed under a Creative Commons Attribution-NonCommercial 3.0 Unported Licence.

Table 8 Effect of pigment by coating modification

Temperature (°C)	Time (min)	Kaolin (%)	*L*	*a*	*b*	*c*	*H*	Tinctorial strength (%)	Flowability (mm)
—	—	—	45.94	48.57	25.60	54.91	27.79	100.0	26
140	180	—	47.69	53.08	24.53	58.48	24.82	141.2	36
140	180	5	45.93	54.99	31.56	63.40	29.85	138.3	39
140	180	10	46.98	55.59	29.78	63.06	28.18	131.7	40
140	180	15	45.74	54.93	31.39	63.16	29.59	128.4	42
150	90	—	45.04	52.91	31.87	61.79	31.08	147.2	31
150	90	5	45.39	54.19	33.06	63.48	31.39	144.5	32
150	90	10	45.01	53.39	31.97	62.23	30.92	139.5	34
150	90	15	46.24	54.73	30.50	62.66	29.13	132.6	35

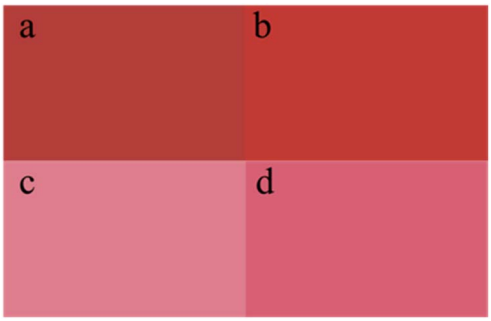

Fig. 10 Color comparison of the modified pigment prepared with Kaolin between α-phase (a: full shade, c: tint shade) and γ-phase (b: full shade, d: tint shade).

gradually decreased with the increasing kaolin concentration. Further, the flowability of the pigment also increased with the increasing kaolin concentration. When the pigment was modified with kaolin, the resulting pigments showed higher colour saturation values than the unmodified pigments, as evidenced by the higher *c* values.

Hydrophilicity of pigments

During the hydrothermal treatment, the polarity and wettability of the pigment particles depend on the heat treatment temperature, heat treatment time, and coating modification. The contact angles of pigments were measured (Table 9). As shown in Table 9, the pigment treated at the same temperature showed a decreasing contact angle with the increasing processing time. Under the isothermal condition, the contact angle of pigments gradually decreased, and the wettability of pigments was improved as the treatment time increased.

The contact angles of kaolin-modified pigments are shown in Table 10. With the increase in the kaolin content, the contact angle decreased, suggesting improved hydrophilicity. Further, when the kaolin content was 15%, the contact angles of pigments obtained at 140 and 150 °C were 71.5° and 76.2°, respectively.

Table 9 Contact angle values of hydrothermal treatment

Temperature (°C)	Time (min)	Contact angle (°)
—	—	89.2
140	60	86.1
140	120	84.5
140	180	82.3
150	45	85.6
150	55	84.2
150	60	82.0
150	90	78.5

Thermal stability of the pigments

The thermal performances of the pristine, hydrothermal-treated, and kaolin-modified pigments were evaluated by the TG-DTG to analyse the changes in thermal stability before and after crystal transformation and kaolin modification. As shown in Fig. 11a, compared with the pristine α-phase pigment, the weight loss curves of the hydrothermal-treated and kaolin-modified pigments moved toward the high-temperature

Table 10 Contact angle values of kaolin modification

Temperature (°C)	Time (min)	Kaolin (%)	Contact angle (°)
140	180	—	82.3
140	180	5	78.2
140	180	10	77.6
140	180	15	71.5
150	90	—	82.0
150	90	5	78.5
150	90	10	77.5
150	90	15	76.2

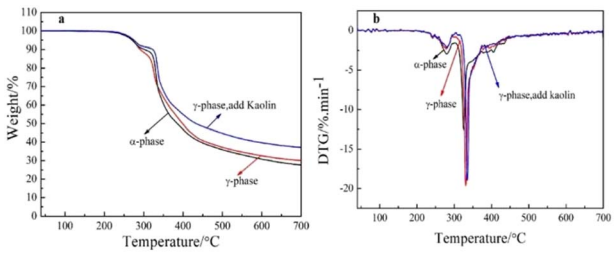

Fig. 11 TG (a) and DTG (b) traces of the α-phase pigment and the γ-phase pigment.

Open Access Article. Published on 02 October 2023. Downloaded on 11/4/2025 12:38:13 AM.
This article is licensed under a Creative Commons Attribution-NonCommercial 3.0 Unported Licence.

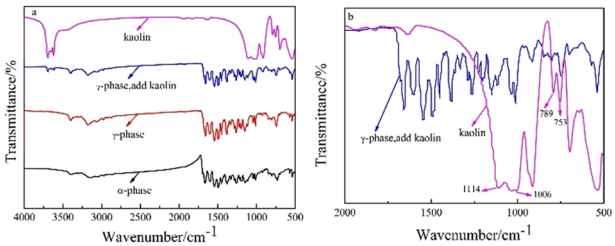

Fig. 12 Infrared spectra of α-phase pigment, γ-phase pigment and pigments modified by coating modification (a) and enlarge image (b).

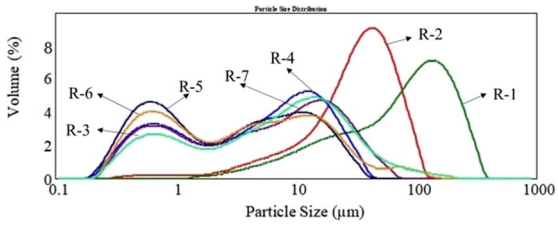

Fig. 13 The particle size distribution histograms of pigment Red 170.

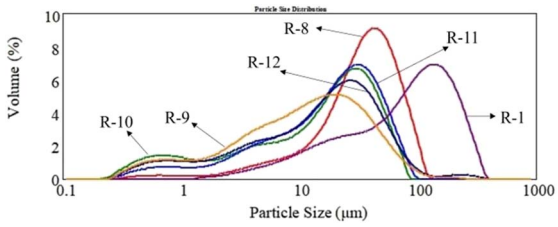

Fig. 14 The particle size distribution histograms of pigment Red 170.

region, and decreased weight loss rates were observed. The weight loss rate of kaolin-modified pigment was the slowest. In addition, in the DTG curves (Fig. 11b), the decomposition temperature of α-phase pigment Red 170 was 330 °C, while that of the pigment after transformation was 340 °C. The comparison showed that the hydrothermal treatment improved the thermal stability of pigment Red 170, and the decomposition temperature increased by 10 °C. In Fig. 11b, the decomposition temperature of the kaolin-modified pigment was 343 °C, which was 13 °C higher than that of the α-phase pigment. The Si–OH groups in the kaolin tended to form hydrogen bonding with –OH and C═O groups in the pigment Red 170, thus improving the thermal stability of the modified pigment.

FT-IR spectroscopy

The chemical structures of the pristine, hydrothermal-treated, and kaolin-modified pigments were evaluated by FT-IR. As shown in Fig. 12a, the pristine α-phase and hydrothermal-treated γ-phase pigments had similar FT-IR spectra, suggesting that the phase transformation had no significant effect on the chemical structures of pigment Red 170. Considering their significantly different XRD patterns, it is confirmed that the α-phase and γ-phase pigments were homogeneous heterocrystals. After kaolin modification, the absorption peaks of –OH stretching vibration emerged at 3652 and 3667 cm^{-1}. To investigate the interaction between the organic pigment and kaolin, the infrared spectra of kaolin and kaolin-modified pigments were compared in Fig. 12b from 500 to 2000 cm^{-1}. In the spectrum of kaolin, the absorption peaks at 753 and 789 cm^{-1} corresponded to the Si–Si stretching vibrations, and the peaks at 1006 and 1114 cm^{-1} belonged to the Si–O stretching vibrations.[32] In the spectrum of kaolin-modified pigment, the above four peaks disappeared, suggesting kaolin was coated on pigment Red 170, and the characteristic absorption peaks of kaolin were covered.

Particle size and distribution analysis

The particle size distributions of the untreated, hydrothermal-treated, and kaolin-modified pigments are shown in Table 11, Fig. 13, and 14. The untreated pigment had a large particle size and wide size distribution. In contrast, the small particle size (D_{10}), medium particle size (D_{50}), and large particle size (D_{90}) of the pigments after the hydrothermal treatment decreased significantly (Table 11), and the particle size decreased with the increase in the treatment time. In addition, the particle size of the kaolin-modified pigment tended to increase with the amount of kaolin powder but decreased significantly compared

Table 11 Particle size distribution of pigment Red 170

No.	Temperature (°C)	Time (min)	Kaolin (%)	$D(0.1)$/um	$D(0.5)$/um	$D(0.9)$/um
R-1	—	—	—	11.978	85.510	219.815
R-2	140	55	—	7.923	34.691	73.594
R-3	140	120	—	0.598	7.487	32.123
R-4	140	180	—	0.514	5.305	20.434
R-5	140	180	5	0.444	2.976	17.088
R-6	140	180	10	0.486	3.786	23.058
R-7	140	180	15	0.543	6.042	27.785
R-8	150	45	—	8.470	35.644	74.224
R-9	150	90	—	1.938	30.674	94.330
R-10	150	90	5	1.018	17.623	47.762
R-11	150	90	10	2.557	20.058	51.961
R-12	150	90	15	1.488	16.902	52.542

 © 2023 The Author(s). Published by the Royal Society of Chemistry

Open Access Article. Published on 02 October 2023. Downloaded on 11/4/2025 12:38:13 AM. This article is licensed under a Creative Commons Attribution-NonCommercial 3.0 Unported Licence.

with that of the untreated pigment. The inorganic kaolin powder with small particle size (0.2–1 μm) and narrow distribution formed a shell on the organic pigment core. The core–shell structure could inhibit particle growth and prevent particle aggregation during the preparation process.

Conclusion

The isothermal crystallisation kinetics of pigment Red 170 was studied by XRD, and an Avrami index $n \approx 3$ was obtained, indicating that the isothermal crystallisation follows three-dimensional spherical growth. The apparent activation energies were 10.42 and 24.31 kcal mol^{-1} for the incubation period and total transition, respectively. XRD and FT-IR spectroscopy showed that the α-phase and γ-phase of pigment Red 170 were homogeneous and heterocrystals. After the hydrothermal treatment, the tinctorial strength of pigment Red 170 increased by 4–89.5%; the thermal decomposition temperature increased by 10 °C; the particle size, crystallinity, flowability, and hydrophilicity also improved. After kaolin modification, the thermal decomposition temperature of pigment Red 170 increased by 13 °C. The particle size decreased significantly, and the hydrophilicity and flowability were enhanced. The hydrothermal treatment and kaolin modification provide new ways to improve the performance of pigment Red 170 for use in plastics, coatings, and other industries. This study promotes the development of pigments with enhanced colour properties, thermal stability, and processability.

Author contributions

Dongjun Lv: conceptualisation, methodology, investigation, writing, project administration, Xiaolei Zhang: conceptualisation, Zilong Zhang: investigation, writing – original draft, formal analysis, Jiahui Zhang: conceptualisation, Yi Li: investigation, Ruobing Qi: formal analysis, Yuxue Zhang: formal analysis, Jing Tang: formal analysis.

Conflicts of interest

The authors declare that they have no known competing financial interests or personal relationships that could have appeared to influence the work reported in this paper.

Acknowledgements

This work was supported by the Natural Science Foundation of Shandong Province (ZR2020MB134 and ZR2020QB082), TaiShan Industrial Experts program of Shandong Province (No. tscx202211094), the Special Found for major Science and Technology Innovation Projects of DeZhou and Foundation of Dezhou University (2020xjrc106, 2019xjrc306 and 2021xjrc305).

Notes and references

1 I. C. P. Margarit, O. R. Mattos, J. Roberto and J. P. Quintela, *J. Coat. Technol.*, 2001, **73**(914), 61–65.
2 J. Bieleman, *Additives for Coatings*, John Wiley & Sons, New York, 2008.
3 W. C. Reynolds, G. L. Miller and T. W. Rufty, *Crop Sci.*, 2012, **52**(5), 2375–2384.
4 E. Baez, N. Quazi, I. Ivanov and S. N. Bhattacharya, *Adv. Powder Technol.*, 2009, **20**(3), 267–272.
5 J. H. Duan, Y. Q. Feng, W. X. Wang and X. G. Li, *Mater. Res. Innovations*, 2010, **14**(2), 113–118.
6 D. Qu and J. W. Duncan, *J. Cosmet. Sci.*, 2000, **51**(5), 324–325.
7 Z. M. Hao and A. Iqbal, *Chem. Soc. Rev.*, 1997, **26**(3), 203–213.
8 D. J. Lv, Z. Z. Zhang, J. H. Zhang, X. L. Zhang, L. F. Liu, Y. Gong, J. H. Zhao and Y. Li, *RSC Adv.*, 2022, **12**(34), 21859–21864.
9 Y. F. Lan and J. J. Lin, *Dyes Pigm.*, 2011, **90**(1), 21–27.
10 J. J. Yuan, S. X. Zhou, G. X. Gu and L. M. Wu, *J. Sol-Gel Sci. Technol.*, 2005, **36**(3), 265–274.
11 J. J. Yuan, S. X. Zhou, B. You and L. M. Wu, *Chem. Mater.*, 2005, **17**(14), 3587–3594.
12 J. J. Yuan, W. T. Xing, G. X. Gun and L. M. Wu, *Dyes Pigm.*, 2008, **76**(2), 463–469.
13 H. X. Wu, G. Gao, Y. Zhang and S. W. Guo, *Dyes Pigm.*, 2012, **92**(1), 548–553.
14 W. Li, Z. Li, L. J. Yu and L. T. Yang, CHN. Pat., 106833005A, 2017.
15 D. M. Yan, H. J. Xu, C. Zhou, F. J. Wang, D. Liu, J. P. Huang, L. T. Yang, W. C. Xu, D. S. Gong, L. X. Zhang, B. Liu and S. J. Yan, CHN. Pat., 111378296, 2020.
16 P. Erk, *Angew. Chem., Int. Ed.*, 2004, **43**(34), 4393–4394.
17 B. L. Zhang, Z. Z. Zhang, X. N. Fei, Y. C. Gu and L. Yu, *Pigm. Resin Technol.*, 2016, **45**(3), 141–148.
18 O. A. Hakeim, Q. G. Fan and Y. K. Kim, *Pigm. Resin Technol.*, 2010, **39**(1), 3–8.
19 O. Hakeim, A. Arafa, M. Zahran and L. Abdou, *Colloids. Surfaces. A. Physicochem. Eng. Aspects.*, 2014, **447**, 172–182.
20 R. Asami and I. Kiyoto, *Jpn. Pat.*, WO2015015961A1, 2015.
21 D. Nguyen, H. S. Zondanos, J. M. Farrugia, A. K. Serelis, C. H. Such and B. S. Hawkett, *Langmuir*, 2008, **24**, 2140–2150.
22 S. H. Fu and C. H. Xu, *J. Appl. Polym. Sci.*, 2010, **115**(4), 1929–1934.
23 P. Bugnon, *Prog. Org. Coat.*, 1996, **29**(1), 39–43.
24 J. Wu, L. M. Wang, P. Zhao, F. Wang and G. Wang, *Prog. Org. Coat.*, 2008, **63**(2), 189–194.
25 B. Xiao, H. X. Wu and S. W. Guo, *Dyes Pigm.*, 2016, **127**, 87–93.
26 Z. Z. Zhang, B. L. Zhang and X. N. Fei, *J. Tianjin Chengjian Univ.*, 2015, **21**(01), 60–65.
27 X. N. Fei, L. Y. Cao and Y. L. Liu, *Dyes Pigm.*, 2016, **125**, 192–200.
28 C. Y. Zhang, J. W. Li, N. N. Cui, X. F. Yan, Z. W. Xie and D. M. Qi, *Colloids Surf., A*, 2021, **629**, 127409.
29 M. U. Schmidt, D. W. M. Hofmann, C. Buchsbaum and H. J. Metz, *Angew. Chem., Int. Ed.*, 2006, **45**, 1313–1317.
30 R. Warshamanage, A. Linden, H. B. Burgi and D. Chernyshov, *Acta Crystallogr., Sect. A: Found. Crystallogr.*, 2011, **67**, C419.
31 E. E. Finney and R. G. Finke, *Chem. Mat.*, 2009, **21**, 4692–4705.
32 M. Ritz, *Minerals*, 2023, **13**, 11.